Journal of King Saud University – Science 34 (2022) 101967

Contents lists available at ScienceDirect

Journal of King Saud University – Science

journal homepage: www.sciencedirect.com

Original article

Development of a gamma-ray scintillation detector based on blue-emitting oligomers and ZnO nanoparticles

Nassar N. Asemi [a], Mamduh J. Aljaafreh [a,b], Saradh Prasad [a,b], Saad Aldawood [a], Mohamad S. AlSalhi [a,b,*]

[a] Department of Physics and Astronomy, College of Science, King Saud University, Riyadh 11451, Saudi Arabia
[b] Research Chair on Laser Diagnosis of Cancers, Department of Physics and Astronomy, College of Science, King Saud University, Riyadh 11451, Saudi Arabia

ARTICLE INFO

Article history:
Received 10 January 2022
Revised 20 February 2022
Accepted 8 March 2022
Available online 14 March 2022

Keywords:
Conjugated oligomer
ZnO nanoparticles
Gamma-ray detector
Plastic scintillators

ABSTRACT

We report the design of flexible, inexpensive, enduring, and efficient composite scintillation based on polystyrene (PS)/blue-emitting conjugated oligomer (CO)/ZnO nanoparticles. The oligomer utilized was 1,4-bis(9-ethyl-3-carbazo-vinylene)-9,9-dihexyl-fluorene (ADS086BE or BECV-DHF). Polystyrene was used as a matrix, and ZnO NPs were used as γ-ray stoppers. The formation of blends was analyzed using X-ray diffraction (XRD) and EDS. Field emission scanning electron microscopy (FE-SEM) images showed micron-sized bun (nearly square)-shaped domains, noodle-like structures, and submicron-sized domains with square-shaped nanosized domains for PS, PS/BECV-DHF, and PS/BECV-DHF/ZnO scintillator samples. The optical properties show that PS/BECV-DHF and PS/BECV-DHF/ZnO had absorption peaks at 350 and 375 nm and fluorescence peaks at 455 nm and 475 nm, respectively. The fabricated scintillators were coupled to the R6094 Hamamatsu Photomultiplier and gamma data acquisition system based on a multichannel analyzer (MCA). Gamma spectra were measured via three gamma-ray sources, Am-241, Cs-137 and Co-60. The results show better scintillation counting in the fabricated PS/BECV-DHF/ZnO than PS/BECV-DHF and the PS sample reference samples.

1. Introduction

Gamma-ray (γ-ray)-detecting plastic scintillators are actively researched due to their ease of fabrication, excellent quantum yield, and low cost. The scintillation detector is one of the most extensively used particle detection systems. It uses materials to emit photons upon encountering a nuclear particle or radiation (L'Annunziata, 2012; VOSE, 1980). Scintillation is rare, since most high-energy photons or particles are naive to interact with ordinary materials. The high-energy particle detection design is based on understanding the interactions between particles and the material; hence, these interactions depend on the properties of the particle and the detector. When a material is bumped by charged particles, they excite the electron to the upper excited state, and the de-excitation of the electrons produces luminescence; this mechanism is known as scintillation. These scintillations can be amplified using a photomultiplier and electronically collected to provide information about the incident radiation (Kharzheev, 2015; Leo, 1994). Ionization radiation detection has been investigated for over 60 years and has many beneficial applications, such as medicine, industry, agriculture, and advanced scientific research (Knoll et al., 2000).

In particular, the medical field is one of the most critical applications of scintillation detectors such as diagnostics (Russo, 2018), positron emission tomography (PET) (Bailey et al., 2005), and gamma cameras(Sánchez et al., 2004). Scintillators are also used in various applications, such as security radiation detectors, particle detectors, new energy resource discovery, and nuclear cameras (Anger, 1958).

The requirement for low-cost and dependable radiation detectors has triggered the important development of new radiation detector materials. Since. In the mid-20th century, organic scintillation counters have been widely utilized for radiation detection (Birks, 1954; Iwanowska et al., 2011; Perego et al., 2021). Due

* Corresponding author at: Department of Physics and Astronomy, College of Science, King Saud University, Riyadh 11451, Saudi Arabia.
E-mail address: malsalhi@ksu.edu.sa (M.S. AlSalhi).

Peer review under responsibility of King Saud University.

Production and hosting by Elsevier

https://doi.org/10.1016/j.jksus.2022.101967
1018-3647/

to the detection efficiency, fast decay time, and fabrication simplicity, organic scintillators are attractive materials for many applications, such as scientific research, industry, and medicine (Leo, 1994). Aromatic hydrocarbon compounds with a benzenic cycle make up organic scintillators. The molecular effect is the mechanism of light emission in organic scintillators. De-excitation of a primary fluorescent material makes bands of ultraviolet (UV) light emitted when the molecular levels are excited (Leroy and Rancoita, 2016). There are three main types of organic scintillators: anthracene crystals, naphthalene liquids, and polymers. Their densities are 1.03–1.25 g/cm^3 depending on the scintillating material in use.

Flexibility is one of the most notable features of plastics, which can be easily formed and machined using conventional methods. Commercially, plastics are found in a broad range of sizes and shapes, and they are relatively affordable (Leo, 1994). Polymers are preferred in various applications due to their optical transparency. Furthermore, polymer devices are low-cost and disposable (Galceran et al., 2013). PS is a semi-transparent polymer often used for light scintillation and gamma radiation detection (Oktar et al., n.d). Compared to other synthetic polymers, PS is extremely radiation-resistant, exhibits radioluminescence, and is widely used as a base for plastic scintillators due to its valuable properties, such as transparency, resistance to aggressive media, and goodness dielectric material (Nurmukhametov et al., 2007). Conjugated oligomers have the advantages of both small molecules and polymers, since they are polymer-like repetitive units but limited to fewer than ten monomers. Furthermore, conjugated oligomers can self-assemble and retain the chemical properties of the parent conjugated polymer, which makes them ideal for organic optics components and optoelectronic devices (Ishikawa and Manabe, 2006; Lin and Zhan, 2016; Prasad et al., 2020). ADS086BE with excellent optical properties are used as a laser gain medium (Aljaafreh et al., 2019a; Aljaafreh et al., 2019b) and a wavelength shifter for organic light-emitting diodes (OLEDs), which are suitable for use in the sensitive region of the photomultiplier photocathode. Combining conjugated oligomers with PS improves the scintillation performance (Kim et al., n.d).

Furthermore, nanomaterials with mid to high Z numbers can help as a high-energy particle stopping material. Considering sub-nanosecond decay times, medium density (5.6 g/cm^3), and potential high light output, ZnO nanoparticles can be suitable for scintillator design (Yanagida et al., 2010). Zinc oxide (ZnO) is an excellent material for various applications (Özgür et al., 2005; Venevtsev et al., 2021). ZnO has an energy gap (Eg) of 3.3 eV at ambient temperature, which makes it a broader bandgap semiconductor (Özgür et al., 2005). There are two types of ZnO emission: ultraviolet emission on the edge of ZnO fundamental absorption in the range of 380–400 nm and green luminescence in the spectral range of 450–650 nm, which makes it ideal for applications that need fast counting (Venevtsev et al., 2021). As a high light-harvesting material, ZnO nanoparticles can be coupled with scintillating agents due to their energy transfer capabilities (Makhal et al., 2010).

In this preliminary investigation, we report a simple design of low-cost plastic scintillators that use an oligomer BECV-DHF, ZnO nanoparticles, and a PS matrix. For this purpose, various PS/BECV-DHF/ZnO-type scintillators were tested under three different gamma radiation sources. Optical properties such as absorption and photoluminescence were measured for the fabricated scintillators. The morphology of the samples was studied through XRD, FE-SEM) images and EDS. This study can be the first report based on an oligomer, which is nanoparticle ZnO, in a PS matrix as a gamma-ray detector.

2. Experimental

2.1. Materials

The molecular structures of polystyrene (PS) and the conjugated oligomer BECV-DHF are shown in Fig. 1(a and b). PS and BECV-DHF were obtained from Merck (Sigma Alrich), FL, USA, and American Dye Source (Montreal, Quebec, Canada) and used without further processing. The molecular masses of PS and BECV-DHF are 60000 g mol^{-1} and 773.12 g mol^{-1} from the datasheet and cross-checked with thin-film chromatography.

The synthesis of ZnO is described in Section 2.2. The ZnO nanoparticles have a mean size of 40 nm with 80% particles within the size range of 20–65 nm, and the distribution range was 5–150 nm.

2.2. Synthesis of ZnO nanoparticles

A stock solution of Zn $(CH_3COO)_2{\cdot}2H_2O$ (0.1 M) was prepared in 50 mL of methanol under stirring. To the above solution, 25 mL of NaOH 0.2 M solution was added to methanol under non-stop stirring. The pH was adjusted to 8, and the resulting solution was transferred to the Opti-sense nanoparticle synthesizer (a Teflon lined sealed stainless-steel autoclave); the temperature was set to 120 °C for 20 hr. The resulting product is filtered and dried.

2.3. Scintillator sample preparation

We prepared three samples with the same shape and thickness (1.5 mm), as shown in Fig. 2.

The scintillator samples were prepared using a blending method. Active materials such as BECV-DHF and ZnO were dispersed to form concentrated solutions and later dispersed into a PS matrix (dissolved in toluene), ultrasonicated for 30 min and kept at room temperature for 24 hr to form a solid. ***Sample 1 (S1) was prepared as*** 1 g of PS dissolved in four mL of toluene. The mixture was sonicated for two hours before being placed in a silicone mold for 24 hr to solidify the mixture. ***Sample 2 (S2)***: Thirty milligrams of BECV-DHF was dissolved in 1 mL of toluene and subsequently dispersed into the PS matrix. The composite was sonicated for 10 min and dropped into a mold. ***Sample 3 (S3)***: Ten milligrams of ZnO nanoparticles dissolved in 1 mL of

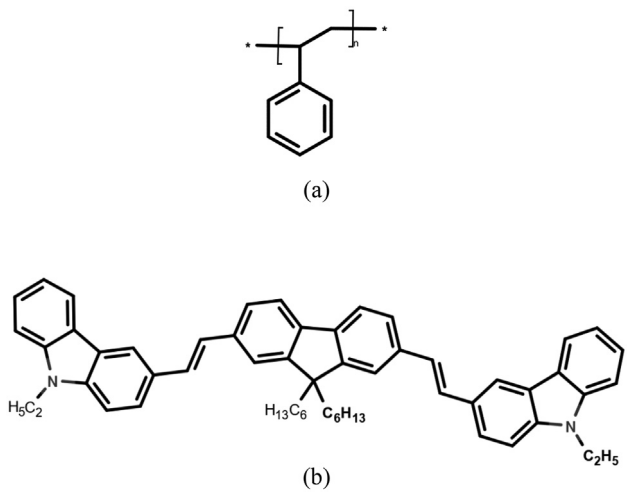

Fig. 1. (a) Molecular structure of polystyrene (PS) and (b) conjugated oligomer BECV-DHF.

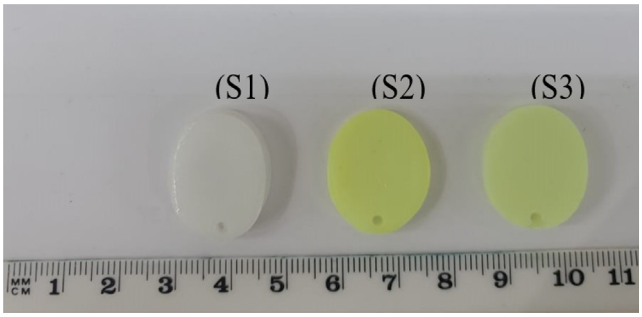

Fig. 2. Fabricated scintillators from left to right PS, PS/BECV-DHF, and PS/BECV-DHF/ZnO.

toluene and sonicated for two hours then placed in the PS-BECV-DHF matrix, and the combination was sonicated for 10 min before being mixed into the composite. The absorption and photoluminescence spectra of the prepared samples were recorded using a spectrophotometer and spectrofluorometer from Perkin Elmer company with ranges of 300–1000 nm and 300–800 nm, respectively. High resolution images of samples were obtained using a JSM-7600F Schottky Field Emission Scanning Electron Microscope (FE-SEM) and the instrument is used for Energy Dispersive Spectroscopy (EDS).

3. Results and discussion

3.1. Structural analysis

XRD of the prepared samples was accomplished on an X-ray diffractometer instrument with copper radiation (wavelength = 1. 5418 Å) and a scanning angle (2θ = 10°–90) from Miniflex 600, Rigaku, Japan. XRD patterns of all three samples are shown in Fig. 3. PS was involved in the hump found at 2θ = 19°, which implies that PS was made of amorphous materials. Similarly, PS/ BECV-DHF showed a broad peak that corresponded to the amorphous state of BECV-DHF, and there were no other significant peaks. PS/ BECV-DHF/ZnO NPs peaked at 2-theta values of 31.80°, 34.46°, 36.40°, 47.44°, 56.46°, 62.78°,66.56°, 68.04°, 69.04° and 72.34°which corresponded to (100), (002), (101), (102), (110), (103), (200), (112), (201), and (004), respectively, and showed a broad peak corresponding to BECV-DHF, which indicates the formation of PS/ BECV-DHF/ZnO.

EDS spectra were obtained using an FE-SEM. EDS spectrum of (i) PS, (ii) PS/BECV-DHF, and (iii) PS/BECV-DHF/ZnO nanocomposite samples are shown in Fig. 4. PS and PS/ BECV-DHF showed peaks from carbon (C) and nitrogen (N). The platinum peak is due to the tiny coating of Pt for 10 s to improve the conductivity of the samples. However, the sample PS/ BECV-DHF/ZnO sample showed peaks of Zn, C, and O, which confirms the presence of ZnO nanoparticles in the sample.

3.2. Morphological analysis

Fig. 5 illustrates the FE-SEM images of (a) PS, (b) PS/BECV-DHF, and (c) PS/BECV-DHF/ZnO. The PS domains are colorized green; similarly, some oligomer patches and ZnO nanoparticles are colorized blue and red, respectively. Fig. 5(a) shows that the domains of PS were almost square-shaped with an average size of 794 nm and a standard deviation of 170 nm. The relatively large domain sizes indicate that PS was submicroscale in pure films made by dissolving the PS pellets in toluene solvent. Fig. 5(b) depicts nano- to submicron-size (length) nested wire-like structures for PS/ BECV-DHF composite thick films (disc).

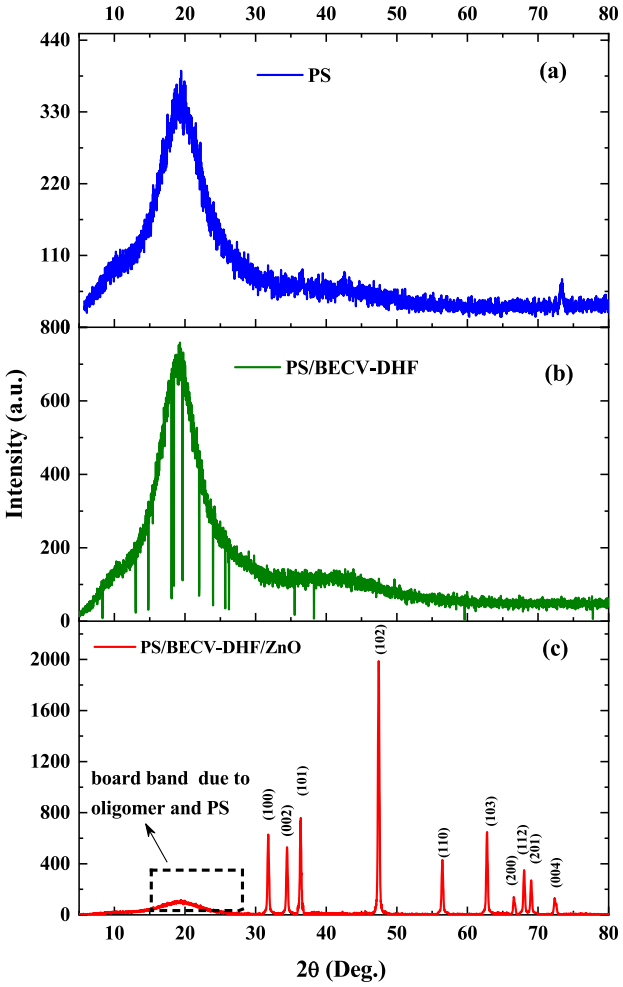

Fig. 3. (a) X-ray diffraction patterns of the (i) PS sample, (ii) PS/BECV-DHF sample and (iii) PS/BECV-DHF ZnO nanocomposite sample.

The average length of the nanowire was 224 nm, whereas the nanowire was only 31 nm wide. The image also shows that PS domains became nanosized with an average size of 66 nm; it looks like the head of the wires. Fig. 5(c) illustrates a highly dispersed composite of a PS/ BECV-DHF/ZnO thick film (disc). The domains of PS also indicate ZnO nanoparticles covered with PS/ BECV-DHF, and the average size of square-shaped ZnO nanoparticles was approximately 39 nm. The process of including BECV-DHF and ZnO into the PS matrix reduces the submicron-sized PS into nanosized domains; similarly, it greatly reduces the gap between domains from 250 nm to 10 nm. All of these changes make PS/ BECV-DHF/ZnO a more suitable composite material for γ-ray scintillation because ZnO has a high Z number, which can help stop γ-rays. The presence of CO on the edges of the domains can also increase the emission from the plasmonic effect. CO is emitted in the blue region, where the PMT tube has the most significant quantum yield.

3.3. Optical properties

Fig. 6(a) shows the absorption spectra of pure PS and composites of PS, i.e., (i) PS, (ii) PS/BECV-DHF, and (ii) PS/BECV-DHF/ZnO. The absorption spectrum of PS shows a peak at 354 nm, and PS/ BECV-DHF shows a peak at 403 nm and a shoulder at a shorter wavelength of approximately 367 nm. PS/BECV-DHF/ZnO shows a high optical absorbance of 1.54 (units) with a peak at approxi-

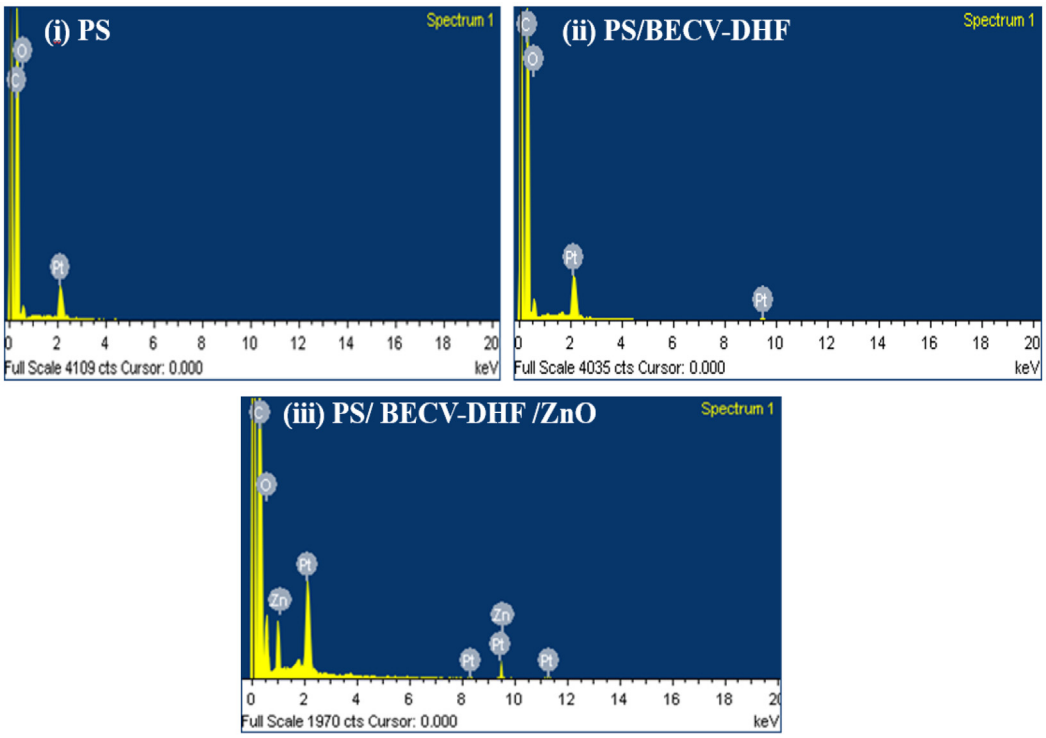

Fig. 4. Energy-dispersive X-ray (EDX) spectroscopy of (i) PS, (ii) PS/BECV-DHF, and (iii) PS/BECV-DHF/ZnO nanocomposite samples.

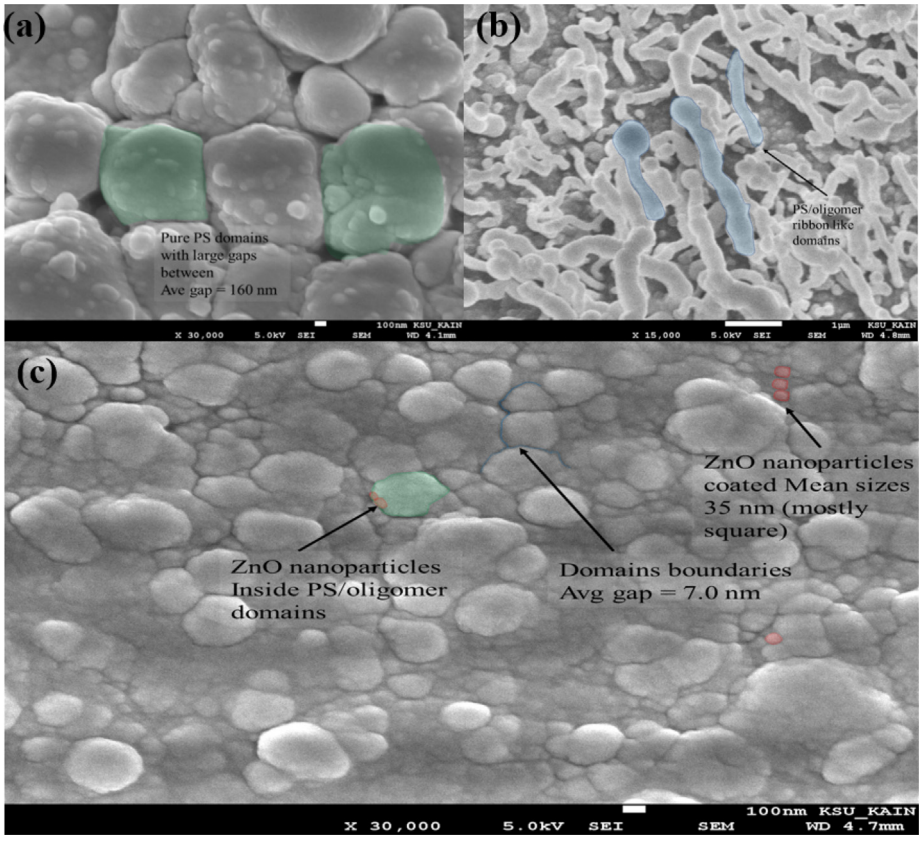

Fig. 5. FE-SEM image of (a) PS, (b) PS/BECV-DHF, and (c) PS/BECV-DHF/ZnO. The PS domains are colorized green; similarly, some oligomer patches and ZnO nanoparticles are colorized blue and red, respectively.

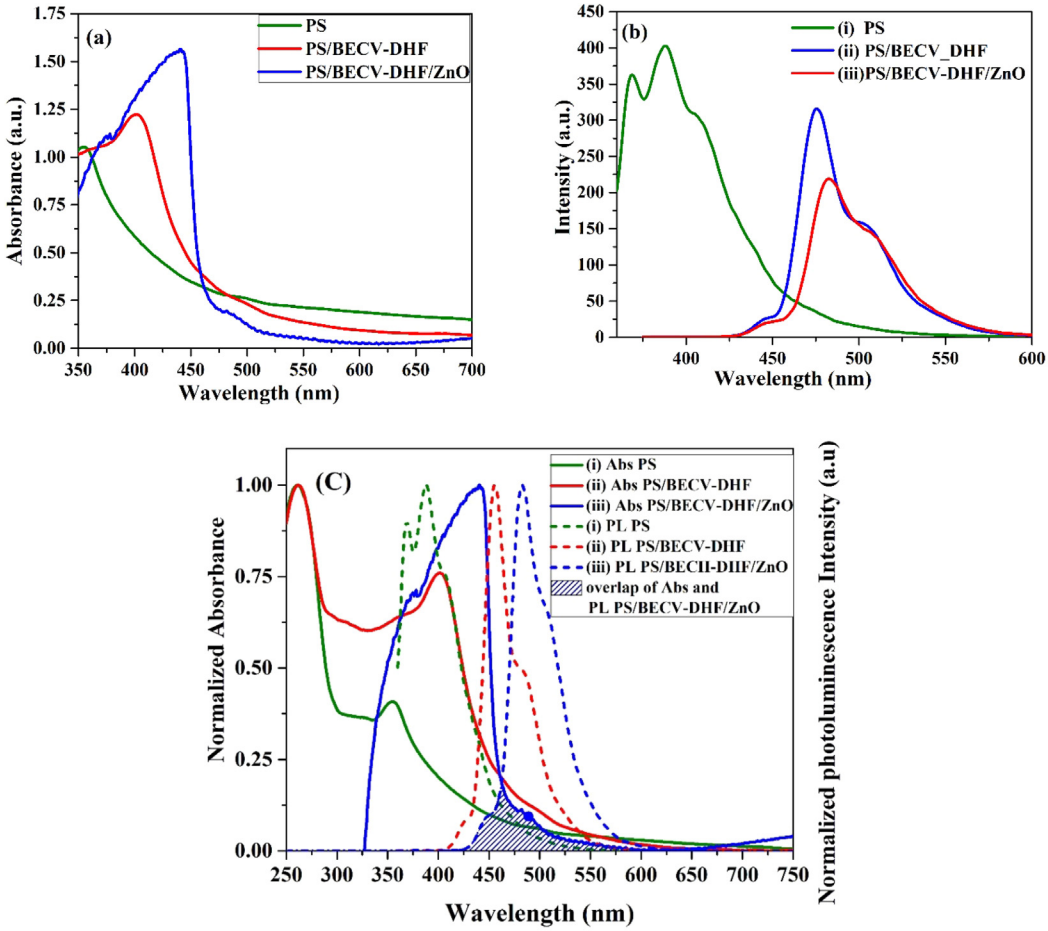

Fig. 6. (a) Absorption and (b) photoluminescence spectra and (c) normalized absorbance (solid line) and photoluminescence spectra of (i) PS, (ii) PS/BECV-DHF, and (ii) PS/ BECV-DHF/ZnO.

mately 438 nm and a shoulder at approximately 375 nm. The absorption spectra show that if a γ-ray is stopped by ZnO and shifted to UV or blue photons, the composite material can readily absorb it.

Fig. 6(b) shows the photoluminescence spectra of (i) PS, (ii) PS/ BECV-DHF, and (iii) PS/ BECV-DHF/ZnO. The photoluminescence profile of PS shows two peaks at 368 nm and 388 nm and a shoulder at 407 nm. Features such as the two peaks and shoulder can be attributed to the vibrational transition of PS at $S_{0\text{-}0}$, $S_{0\text{-}1}$, and $S_{0\text{-}2}$. Similarly, PS/ BECV-DHF shows two peaks at 414 nm and 433 nm and a longer wavelength at 451 nm. PS/BECV-DHF/ZnO shows a high photoluminescence intensity of 315 (a.u.) with a peak approximately 476 nm and a shoulder approximately 503 nm. Here, $S_{0\text{-}0}$ is dumbed, but the $S_{0\text{-}1}$ and $S_{0\text{-}2}$ vibrational bands correspond to these peaks and the shoulder. Fig. 6(c) shows the normalized absorbance and photoluminescence of (i) PS, (ii) PS/ BECV-DHF, and (iii) PS/ BECV-DHF/ZnO. The spectral overlap between absorption and photoluminescence in PS/ BECV-DHF and PS/ BECV-DHF/ ZnO was small (shown as shaded blue lines). Hence, triplet trapping states or nonradiation pathways are almost not present. Hence, the vibration bands are a fast absorption-photoluminescence cycle system, and the response of scintillators becomes fast.

3.4. Gamma spectroscopy

Three different samples were fabricated for scintillation: PS, PS doped with BECV-DHF, and PS doped with BECV-DHF-ZnO, as presented in Fig. 2. The unshielded gamma-emitting sources were Am-241, Cs-137, and Co-60, with activities$1.1\mu c, 2.8\mu c,$ $and 1.1\mu c$respectively. Am-241 is considered a low-gamma-energy source, Cs-137 is a relatively higher-gamma-energy source, and Co-60 that emits higher gamma energy than the other two sources. The samples were wrapped in 0.5-mm-thick Teflon to increase the reflection and subsequently coupled to a photomultiplier (PMT) (Ghorbani et al., 2019). A thin film of spatial silicon grease was spread over the PMT window to reduce the light emission refraction index (Mapelli, 2011). The signal from the detector was a tail wave shape with an average amplitude of −30 mV. Then, the signal was sent to the amplifier and fed to the multichannel (MCA) with a dynamic range of 0 to ± 10 V, rise time greater than 0.1 μs, and a resolution of 13-bit fast analog-to-digital converter

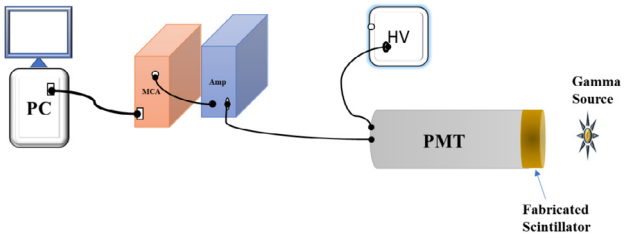

Fig. 7. A diagram of the experimental setup to measure the gamma spectra using the fabricated scintillators.

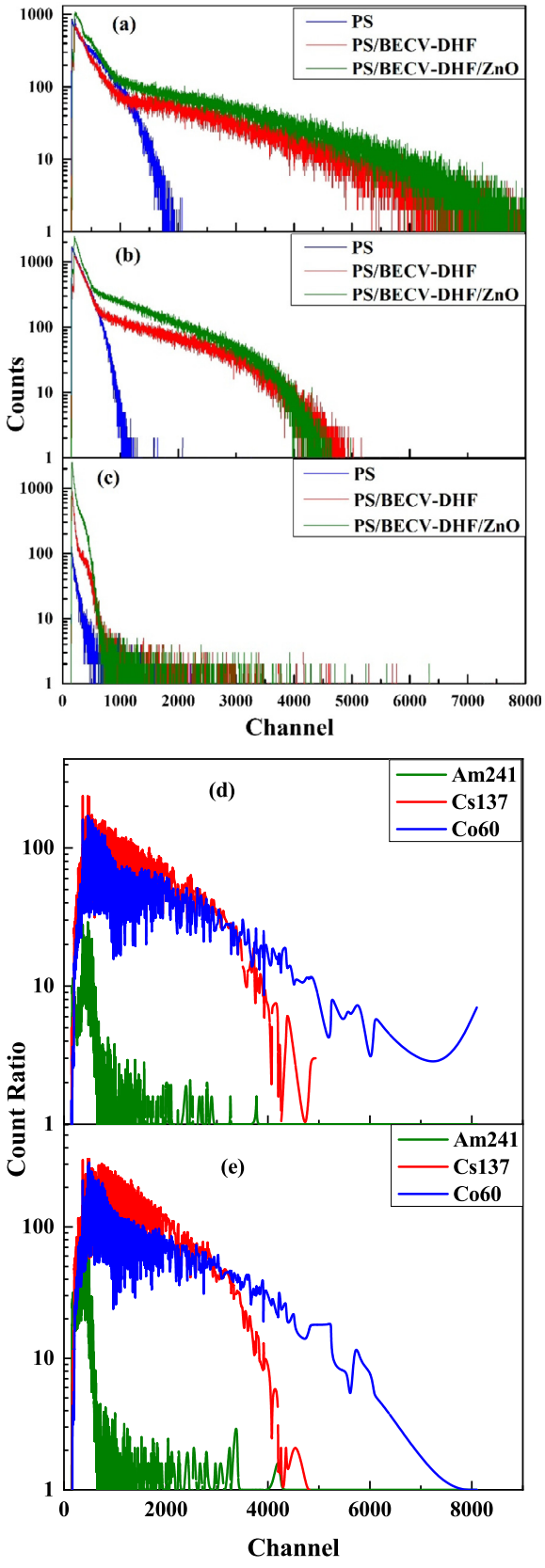

Fig. 8. Gamma spectra of PS, PS/BECV-DHF and PS/BECV-DHF/ZnO fabricated samples using three gamma sources: (a) Co-60 (b) Cs-137, and (c) Am-241, (d) count ratio plot from the gamma spectra, the ratio is determined by the total counts for (PS/BECV-DHF) divided by the pure PS sample, and (e) count ratio plot for (PS/ZnO/BECV-DHF) divided by the pure PS sample.

ADC (8192 channels) to digitize the pulses in a multichannel memory. The MCA is subsequently connected to a PC by USB for signal processing using the N957 Demo software (N957 - 8k Multi-Channel Analyzer - CAEN - Tools for Discovery, n.d). Then, the samples were exposed to gamma sources, and measurements for the samples were taken for 2 h for each gamma source. The experimental setup of the experiment is shown in Fig. 7.

A Hamamatsu photomultiplier tube (R6094 PMT) (R6094 Hamamatsu PHOTOMULTIPLIER TUBES ChipFind Datasheet Archive | ChipFind.net, n.d.) was employed as a photodetector. According to the datasheet, it has a quantum efficiency between ~28% at 400 nm and ~17% at 500 nm, which is compatible throughout the emission wavelength range of samples.

Fig. 8 shows gamma spectra of PS, PS/BECV-DHF, and PS/BECV-DHF/ZnO fabricated samples using three gamma sources: (a) Co-60, (b) Cs-137, and (c) Am-241. We observe noticeable improvements in the count rate after BECV-DHF has been added to the PS matrix. In most cases, the reason is the possibility of energy transfer between the two components BECV-DHF and PS (Tam et al., 2018). The scintillation enhancement of gamma becomes better after embedding ZnO nanoparticles into the scintillating organic matrix primarily because of the higher attenuation of ZnO nanoparticles for gamma energy (Alsayed et al., 2019). Fig. 8(d and e) show the count ratio for the gamma spectra, which is the total counts of the PS/BECV-DHF and PS/BECV-DHF/ZnO samples, respectively, divided by the total count of the pure PS sample. The ratio indicates that there is an enhancement in the light yield. This enhancement exceeded 100 times in some energy regions of the PS-BECV-DHF sample using Co-60 and Cs-130 sources. The count ratio was lower using Am-241, which means that the enhancement appears clearly for mid-range and high energies (Cs-137 and Co-60) compared to the low energies (Am-241). PS/BECV-DHF/ZnO showed a slightly better light yield count ratio than PS/BECV-DHF, especially at low energies under 2000 channels. The output of PS/BECV-DHF can be attributed to the efficient wave shifting capability of the BECV-DHF oligomer. The improved output attained in PS/BECV-DHF/ZnO can be attributed to the stopping power of ZnO nanoparticles and the improved energy transfer from PS and ZnO to the BECV-DHF oligomer (Kim et al., n.d).

The scintillation count rate (count per minute (CPM)) and intrinsic efficiency of the fabricated samples are shown in Table 1. The intrinsic efficiency calculated in the table is the ratio of the number of photons detected by the samples to the number of photons incident on the sample surface (Knoll et al., 2000). PS/BECV-DHF/ZnO shows an increased intrinsic efficiency of 0.94% compared to PS/BECV-DHF (0.60%) and PS (0.50%) for the Co-60 gamma source.

A comparison of gross count rate per microcurie (CPM/ μc) of the samples using the gamma-ray sources is displayed in Fig. 9. The (CPM/ μc) increased with the addition of BECV-DHF to PS. The addition of ZnO nanoparticles to the BECV-DHF-PS mixture significantly increased the overall performance of the material. The PS/BECV-DHF/ZnO sample showed a reasonable (CPM/ μc) of counts up to 1500 CPM/ μc for Cs-137 and up to 3300 CPM/ μc for Co-60, which is double that by the same gamma sources for the PS sample. For the Am-241 gamma source, PS/BECV-DHF/ZnO and PS/BECV-DHF have significantly improved CPM/ μc compared to the pure PS sample. The difference in CPM/μc for different sources is almost due to the difference in gamma source activities and different responses of the samples, which vary according to the energies of the gamma-ray sources.

Table 1
Am-241, Cs-137, and Co60 were used as gamma sources for two hours exposing the different scintillator samples, PS, PS/BECV-DHF, and PS/BECV-DHF/ZnO.The Gross count rate CPM were estimated from the total gross divided by 120 min. and the uncertainties in the count rates were calculated by divided the square root of the total gross counts by the live time (120 min).

Type of sample	Type of sample	Gamma sources		
		Am241	Cs137	Co60
Count rate (CPM)	PS	59.90 ± 0.7	1882 ± 4.0	1638 ± 3.7
	PS/BECV-DHF	390.0 ± 1.8	2599 ± 4.7	1974 ± 4.0
	PS/BECV-DHF/ZnO	1177 ± 3.1	4386 ± 6.0	3072 ± 5.1
Intrinsic efficiency	PS	0.02%	0.19%	0.50%
	PS/BECV-DHF	0.15%	0.26%	0.60%
	PS/BECV-DHF/ZnO	0.45%	0.44%	0.94%

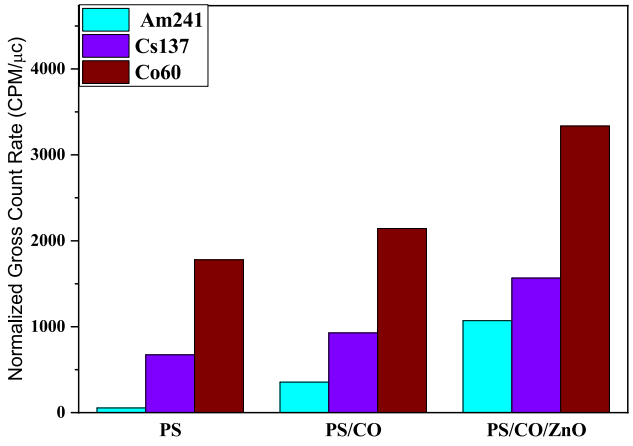

Fig. 9. Gross count rate per minute per μc (CPM/μc) of the fabricated scintillators (PS), (PS/BECV-DHF) and (PS-BECV-DHF/ZnO).

4. Conclusion

In this preliminary report, we used a simple blend method to fabricate three types of flexible plastic scintillators for γ-ray detection. The samples were manufactured with a thickness of 1.5 mm for each sample and ellipse shapes with semi-major axis a = 12 mm and semi-minor axis b = 9 mm. These fabricated samples were sliced and polished on the surface. The XRD and EDX spectra confirm the PS/BECV-DHF and PS/BECV-DHF/ZnO formation. Morphological analysis through FE-SEM images reveals the nanowire formation of the PS/BECV-DHF composite and the formation of a hybrid composite of the PS polymer, BECV-DHF oligomer and ZnO nanoparticles. Three standard gamma ray sources were used to evaluate the characteristics of the fabricated scintillators. The pulse spectra were measured via a photomultiplier, amplifier, high voltage power supply, and MCA. PS/BECV-DHF/ZnO showed the best scintillation counting among the studied samples with a gross count rate (CPM) above 4000 for the Cs-137 gamma source, which were more than double those of the pure polystyrene sample. To improve the light output in the future, other heavy nanoparticles and new oligomer wavelength-shifter materials will be added. These materials are expected to enhance the properties of the scintillator, including ligands containing polymerizable groups, which will help prevent the nanocrystal aggregation in polystyrene-based composites.

Declaration of Competing Interest

The authors declare that they have no known competing financial interests or personal relationships that could have appeared to influence the work reported in this paper.

Acknowledgement

The authors are grateful to the Deanship of Scientific Research, King Saud University for funding through Deanship of Scientific Research Chairs.

References

Aljaafreh, M.J., Prasad, S., AlSalhi, M.S., Alahmed, Z.A., 2019a. Ultrafast dynamics of laser from green conjugated-oligomer in solution. Polymer (Guildf). 169, 106–114. https://doi.org/10.1016/J.POLYMER.2019.02.022.

Aljaafreh, M.J., Prasad, S., AlSalhi, M.S., Alahmed, Z.A., Al-Mogren, M.M., 2019b. Optically pumped intensive light amplification from a blue oligomer. Polymers (Basel). 11, 1534.

Alsayed, Z., Badawi, M.S., Awad, R., Thabet, A.A., El-Khatib, A.M., 2019. Study of some gamma ray attenuation parameters for new shielding materials composed of NANO ZnO blended with high density polyethylene. Nucl. Technol. Radiat. Prot. 34, 342–352. https://doi.org/10.2298/NTRP190718033A.

Anger, H.O., 1958. Scintillation camera. Rev. Sci. Instrum. 29 (1), 27–33.

Bailey, D.L., Townsend, D.W., Valk, P.E., Maisey, M.N. (Eds.), 2005. Positron Emission Tomography. Springer-Verlag, London.

Birks, J.B., 1954. Scintillation counters. Soil Science 77 (2), 171.

Galceran, M., Pujol, M.C., Carvajal, J.J., Mateos, X., Formentín, P., Pallarès, J., Marsal, L.F., Park, K.H., Rotermund, F., Kim, K., Aguiló, M., Díaz, F., 2013. New microarchitectures of (Er, Yb):Lu2O3 nanocrystals embedded in PMMA: Synthesis, structural characterization, and luminescent properties. Nanoscale Res. Lett. 8, 1–8. https://doi.org/10.1186/1556-276X-8-385/TABLES/2.

Ghorbani, P., Sardari, D., Azimirad, R., Hosntalab,, Mohammad,, 2019. Experimental study of a large plastic scintillator response with different reflective coverings based on digital pulse processing method. J. Radioanal. Nucl. Chem. 321, 481–488. https://doi.org/10.1007/s10967-019-06596-5.

Ishikawa, S., Manabe, K., 2006. Repetitive two-step method for oligoarene synthesis through rapid cross-coupling of hydroxyphenylboronic acids and anhydrides. Chem. Lett. 35 (2), 164–165.

J. Iwanowska L. Swiderski M. Moszynski T. Szczesniak P. Sibczynski N.Z. Galunov N. L. Karavaeva Neutron/gamma discrimination properties of composite scintillation detectors J. Instrum. 6 07 2011 P07007 P7007.

Kharzheev, Y.N., 2015. Scintillation counters in modern high-energy physics experiments. Phys. Part. Nucl. 46, 678–728.

Kim, D.G., Lee, S., Kim, Y.H., Seon, J., Kim, Y.K., n.d. Performance of 3D Printing Plastic Scintillator by Applying OLED Wavelength Shifter. Trans. Korean Nucl. Soc. Autumn Meet. Gyeongju.

Knoll, G.E., Arbor, A., Wiley, J., 2000. Radiation Detectibn and Measurement. .

L'Annunziata, M.F., 2012. Handbook of radioactivity analysis. Academic press.

W.R. Leo Techniques for Nuclear and Particle Physics Experiments 1994 Nucl. Part. Phys. Exp Tech 10.1007/978-3-642-57920-2.

C. Leroy P.-G. Rancoita Principles of Radiation Interaction in Matter and Detection 2016 Radiat. Interact. Matter Detect Princ 10.1142/9167.

Lin, Y., Zhan, X., 2016. Oligomer Molecules for Efficient Organic Photovoltaics. Acc. Chem. Res. 49 (2), 175–183.

Makhal, A., Sarkar, S., Bora, T., Baruah, S., Dutta, J., Raychaudhuri, A.K., Pal, S.K., 2010. Dynamics of light harvesting in ZnO nanoparticles. Nanotechnology 21 (26), 265703.

A. Mapelli Scintillation Particle Detectors Based on Plastic Optical Fibres and Microfluidics 2011.

N957 - 8k Multi-Channel Analyzer - CAEN - Tools for Discovery [WWW Document], n.d.

Nurmukhametov, R.N., Volkova, L.V., Klimenko, V.G., Kabanov, S.P., Salov, R.V., 2007. Fluorescence and absorption of a polystyrene-based scintillator exposed to UV laser radiation. J. Appl. Spectrosc. 74, 824–830. https://doi.org/10.1007/S10812-007-0128-2.

Oktar, O., Ari, G., Guenduez, O., Demirel, H., Demirbas, A., n.d. Low cost plastic scintillator by using commercial polystyrene.

Ozgur, U., Alivov, Y.I., Liu, C., Teke, A., Reshchikov, M.A., Dogan, S., Avrutin, V., Cho, S. J., Morko,, H.,, 2005. A comprehensive review of ZnO materials and devices. J. Appl. Phys. 98,. https://doi.org/10.1063/1.1992666 041301.

Perego, J., Villa, I., Pedrini, A., Padovani, E.C., Crapanzano, R., Vedda, A., Dujardin, C., Bezuidenhout, C.X., Bracco, S., Sozzani, P.E., Comotti, A., Gironi, L., Beretta, M., Salomoni, M., Kratochwil, N., Gundacker, S., Auffray, E., Meinardi, F., Monguzzi, A., 2021. Composite fast scintillators based on high-Z fluorescent metal–organic framework nanocrystals. Nat. Photonics 15 (5), 393–400.

Prasad, S., Aljaafreh, M.J., AlSalhi, M.S., 2020. Time-resolved spectroscopy of radiative energy transfer between a conjugated oligomer and polymer in solution. Spectrochim. Acta Part A Mol. Biomol. Spectrosc. 232,. https://doi.org/10.1016/J.SAA.2020.118151 118151.

R6094 Hamamatsu PHOTOMULTIPLIER TUBES ChipFind Datasheet Archive | ChipFind.net [WWW Document], n.d.

Russo, P., 2018. Handbook of X-ray imaging : physics and technology. Handb. X-ray Imaging Phys, Technol.

Sánchez, F., Benlloch, J.M., Escat, B., Pavón, N., Porras, E., Kadi-Hanifi, D., Ruiz, J.A., Mora, F.J., Sebastià, A., 2004. Design and tests of a portable mini gamma camera. Med. Phys. 31, 1384–1397. https://doi.org/10.1118/1.1755570.

Tam, A.K., Boyraz, O., Unangst, J., Nazareta, P., Schreuder, M., Nilsson, M., 2018. Quantum-dot doped polymeric scintillation material for radiation detection. Radiat. Meas. 111, 27–34. https://doi.org/10.1016/J.RADMEAS.2018.02.008.

Venevtsev, I.D., Tarasov, A.P., Muslimov, A.E., Gorokhova, E.I., Zadorozhnaya, L.A., Rodnyi, P.A., Kanevsky, V.M., 2021. Ultraviolet Luminescence of ZnO Whiskers, Nanowalls, Multipods, and Ceramics as Potential Materials for Fast Scintillators. Mater. 2021, Vol. 14, Page 2001 14, 2001. https://doi.org/10.3390/MA14082001.

VOSE, P.B., 1980. CHAPTER 4 - Detection Systems and Instrumentation, in: VOSE, P. B.B.T.-I. to N.T. in A. and P.B. (Ed.), Pergamon International Library of Science, Technology, Engineering and Social Studies. Pergamon, pp. 46–76. https://doi.org/https://doi.org/10.1016/B978-0-08-024924-7.50011-9.

Yanagida, T., Fujimoto, Y., Yoshikawa, A., Yokota, Y., Miyamoto, M., Sekiwa, H., Kobayashi, J., Tokutake, T., Kamada, K., Maeo, S., 2010. Scintillation properties of in doped ZnO with different in concentrations. IEEE Trans. Nucl. Sci. 57, 1325–1328. https://doi.org/10.1109/TNS.2009.2035120.